

# Carbon Paraequilibrium in Austenitic Stainless Steel

G.M. MICHAL, F. ERNST, and A.H. HEUER

Carburization of austenitic stainless steels under paraequilibrium conditions—*i.e.*, at (low) temperatures where there is essentially no substitutional diffusion—leads to a family of steels with remarkable properties: enhanced hardness, resulting in improved wear behavior, enhanced fatigue, and corrosion resistance, and with essentially no loss in ductility. These enhanced properties arise from an enormous carbon solubility, which, absent carbide formation, is orders of magnitude greater than the equilibrium solubility. Using interaction parameters from the latest CALPHAD assessment of the Fe-Cr-Ni-carbon system, the authors have calculated the equilibrium and paraequilibrium carbon solubility in a model Fe-18Cr-12 Ni (wt pct) austenitic steel (essentially a model 316L composition), as well as the carbon solubility in this austenite when paraequilibrium carbide formation occurs (*i.e.*, when carbides form in a partitionless manner). For temperatures in the range 725 to 750 K, the calculations predict a paraequilibrium carbon solubility of  $\sim 5.5$  at. pct. Carburization of 316L stainless steel at these temperatures, however, results in significantly higher concentrations of carbon in solid solution—up to 12 at. pct. Much better agreement with experimental data is obtained by calculating the paraequilibrium carbon solubility using Wagner interaction parameters, taken from the most comprehensive experimental study of this system. The discrepancy between the two predicted solubilities arises because the CALPHAD Cr-carbon interaction parameters are not sufficiently exothermic at the low temperatures used for paraequilibrium carburization. After multiple paraequilibrium carburization cycles, carbide formation can occur. The carbides that form under these conditions do so in a near-partitionless manner (there is modest Ni rejection to the austenite/carbide interface) and have an unusual stoichiometry:  $M_5C_2$  (the Hägg or  $\eta$  carbide).

## I. INTRODUCTION

**HARDENING** of austenitic stainless steels by nitrogen or carbon has been a subject of long-standing interest, as such steels with (traditional) low concentrations of these interstitial solutes are too soft relative to other steels for many applications. Recently,<sup>[1]</sup> low-temperature nitridation and carburization of these have been studied as a potentially effective route to surface hardening. It is possible to dissolve significant quantities of interstitial solutes in single-phase austenite at low temperatures, causing a substantial increase in lattice parameter (the resulting material has been described as “expanded” austenite or S-phase) and concomitant hardening.

In this work, we have focused on low-temperature carburization of a 316L stainless steel, for which remarkable improvements in hardness, wear resistance, fatigue resistance, and corrosion resistance have been realized in a commercially viable process.<sup>[2]</sup> These improvements are accomplished with essentially no attenuation of the inherently good ductility of austenitic stainless steels.

The essence of the approach is shown in Figures 1 and 2. The TTT diagram in Figure 1 concerns the precipitation of  $M_{23}C_6$  in 316 alloys of two different carbon concentrations,

0.31 and 0.10 at. pct,<sup>[3]</sup> while Figure 2 shows the variation of surface hardness with carbon concentration following low-temperature carburization.<sup>[4,5,6]</sup>

Figure 1 shows that carbon can be readily dissolved in 316 austenitic stainless steels at elevated temperatures, but only in small quantities. The carbon solubility increases from 0.10 at. pct at 1130 K to 0.31 at. pct at 1240 K. The corresponding nose of the C-curves likewise varies from  $\approx 1060$  K to  $\approx 1130$  K for the two carbon levels. At lower temperatures, however, the time to initiate precipitation of  $M_{23}C_6$  can be long ( $\approx 1000$  hours at 770 K). The nucleation and growth rates governing carbide formation are not sensitive to the carbon level of the austenite but mainly depend on the diffusivities of substitutional solutes, which are modest at the lower temperature and do not vary much with carbon content. In contrast, the mobility of carbon<sup>[7,8,9]</sup> is still substantial in a certain temperature window below the “C” curves, say between *ca.* 725 and 775 K, enabling *paraequilibrium* carburization in industrially reasonable times. Paraequilibrium was the term first used by Hultgren<sup>[10]</sup> and subsequently by Hillert<sup>[11]</sup> to describe a particular type of metastable equilibrium at temperatures where substitutional solutes are immobile, whereas interstitial solutes are able to diffuse. In a diffusion couple, for example, these conditions would equilibrate the chemical potential of carbon but not the chemical potentials of the substitutional solutes. Although not generally recognized, the paraequilibrium carbon solubility in austenitic stainless steel can be orders of magnitude greater than the equilibrium solubility. It is clear from Figure 2, for example, that carbon levels of up to 12 at. pct can be realized in single-phase austenitic stainless steels.

G.M. MICHAL, F. ERNST, and A.H. HEUER, Professors, are with the Department of Materials Science and Engineering, Case Western Reserve University, Cleveland, OH 44106. Contact e-mail: gmm3@case.edu

This article is based on a presentation made in the “Hillert Symposium on Thermodynamics & Kinetics of Migrating Interfaces in Steels and Other Complex Alloys,” December 2–3, 2004, organized by The Royal Institute of Technology in Stockholm, Sweden.

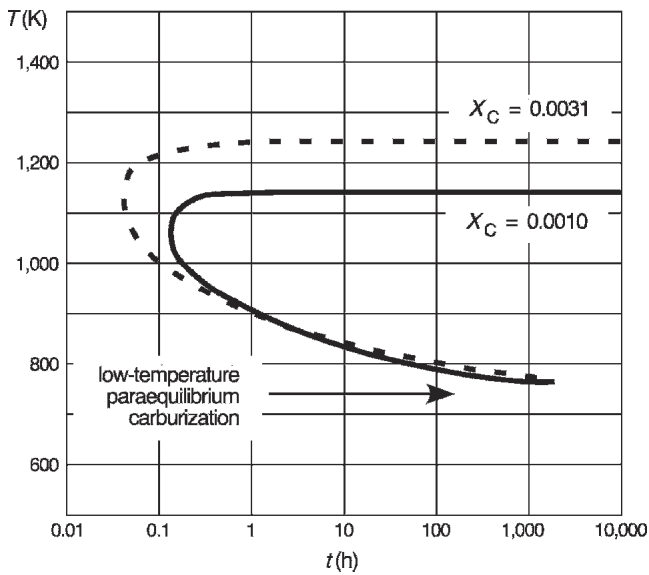


Fig. 1—Time-temperature-transformation diagram to 316 stainless steel alloys solution treated for 1.5 hours at 1533 K, quenched in water and aged.<sup>[3]</sup>

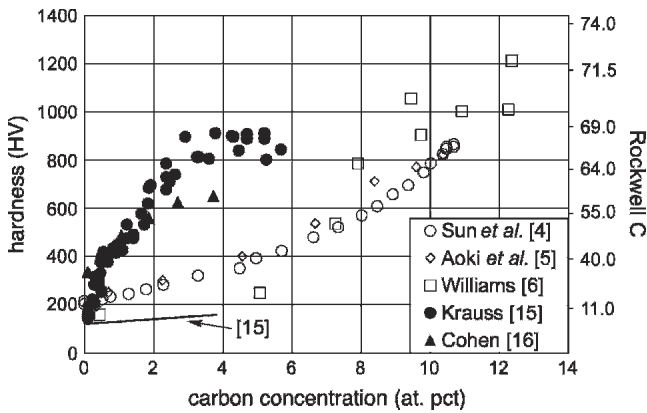


Fig. 2—Vickers hardness as a function of carbon concentration for various steels. The (open symbols) are for 316 austenitic stainless steels, the (filled circles) and (triangles) for martensitic steels. The (solid line) is for *fcc* Fe-Ni-carbon alloys. (Data from References 4, 5, 6, 15, and 16).

We earlier<sup>[12,13]</sup> referred to these high carbon levels as constituting a “colossal” supersaturation; the high carbon levels can lead to surface hardness greater than that found for martensitic steels,<sup>[14,15,16]</sup> as shown in Figure 2. We will return to the issue of hardness in Section IV.

## II. PARAEQUILIBRIUM CARBON SOLUBILITY

We have evaluated the paraequilibrium and equilibrium carbon solubility in a model Fe-18 Cr-12 Ni austenitic stainless steel (concentration in wt pct) using standard solution thermodynamic models. The alloy was assumed to be in contact with an atmosphere having a carbon chemical potential,  $\mu_C$ , equal to that of graphite (*i.e.*, a carbon activity,  $a_C$ , of unity). The “compound energy” or CALPHAD approach to the thermodynamics of solid solutions with multiple sub-lattices is well suited to this purpose.

For such a system,  $\mu_C$  is given by

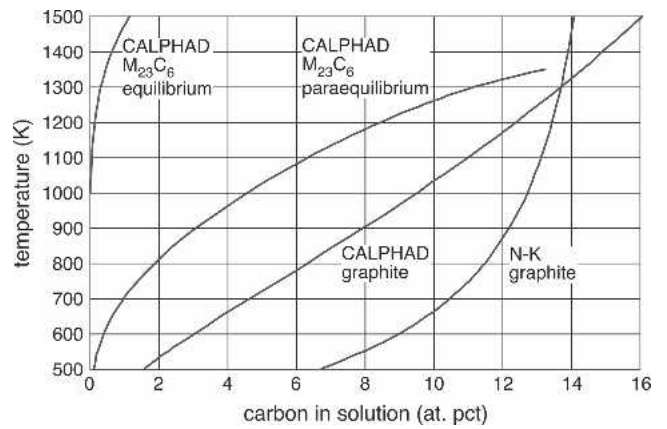


Fig. 3—Carbon solubility in a Fe-18Cr-12Ni (wt pct) austenite as a function of temperature under several conditions.

$$\begin{aligned} \mu_C = & Y_{Cr}({}^0G_{Cr:C}^{fcc} - {}^0G_{Cr}^{hfcc}) + Y_{Fe}({}^0G_{Fe:C}^{fcc} - {}^0G_{Fe}^{hfcc}) \\ & + Y_{Ni}({}^0G_{Ni:C}^{fcc} - {}^0G_{Ni}^{hfcc}) + RT \ln \left[ \frac{Y_C}{1 - Y_C} \right] \\ & + (1 - 2Y_C)(Y_{Cr}^0L_{Cr:C,Va} + Y_{Fe}^0L_{Fe:C,Va}) \\ & + Y_{Cr}Y_{Fe}({}^0L_{Cr:Fe,C} - {}^0L_{Cr:Fe,C} - {}^1L_{Cr:Fe,C}(Y_{Cr} - Y_{Fe})) \\ & + Y_{Fe}Y_{Ni}({}^0L_{Fe:Ni,C} + {}^1L_{Fe:Ni,C}(Y_{Fe} - Y_{Ni}) - {}^0L_{Fe:Ni,Va} \\ & - {}^1L_{Fe:Ni,Va}(Y_{Fe} - Y_{Ni}) - {}^2L_{Fe:Ni,Va}(Y_{Fe} - Y_{Ni})^2) \\ & + Y_{Cr}Y_{Ni}({}^0L_{Cr:Ni,C} - {}^0L_{Cr:Ni,Va} - {}^1L_{Cr:Ni,Va}(Y_{Cr} - Y_{Ni})) \\ & + Y_{Cr}Y_{Fe}Y_{Ni}({}^0L_{Cr,Fe,Ni:C} - {}^0L_{Cr,Fe,Ni,Va}) \end{aligned} \quad [1]$$

$Y_i$  = the site fraction of component  $i$ ,  ${}^0G_j^k$  is the free energy of constituent  $j$  in state  $k$ , and  ${}^nL_{u,v:w;s,t}$  stands for interaction coefficients of order  $n$  for components  $u, v, w, s, t$ .  $h$  in the superscript indicates a hypothetical, nonmagnetic phase. Under paraequilibrium conditions, the site fraction of carbon,  $Y_C$ , at which  $\mu_C$  in Eq. [1] equals  ${}^0G_C^{gra}$  establishes the solubility of carbon in austenite. The curve marked “CALPHAD graphite” in Figure 3 shows the carbon paraequilibrium solubility (in units of at pct, *i.e.*,  $100 \cdot Y_C/(1 + Y_C)$ ) obtained using the CALPHAD parameters taken from the most recent assessment of the Fe-Cr-Ni-carbon system.<sup>[17]</sup>

Under equilibrium conditions, the free energy of the carbide phase,  $M_{23}C_6$ , determines the solubility of carbon in austenite through the relationship

$$G_m^{M_{23}C_6} = 23(Y_{Cr}^{M_{23}C_6} \mu_{Cr} + Y_{Ni}^{M_{23}C_6} \mu_{Ni} + Y_{Fe}^{M_{23}C_6} \mu_{Fe}) + 6\mu_C \quad [2]$$

This equation represents the usual condition for heterogeneous equilibrium, namely that the chemical potentials of Fe, Cr, Ni, and carbon in the *fcc* matrix must equal those in the carbide phase. Using data taken from Reference 17 for the molar free energy of  $M_{23}C_6$  as a function of the composition of its two metal sublattices and the chemical potentials of Cr, Ni, and Fe in the alloy, Eq. [2] was solved for the minimum value of  $\mu_C$ . The corresponding equilibrium solubility of carbon in the model austenitic alloy is plotted as a function of temperature in Figure 3 (the curve

marked "CALPHAD  $M_{23}C_6$  equilibrium"). Along this solvus, the composition of the carbide varies with temperature, becoming increasingly Cr-rich at the lower temperatures. At 1500 K, for example, M corresponds to 72.1 at. pct Cr, 27.0 at. pct Fe, and 0.9 at. pct Ni, while at 500 K, the composition changes to 99.1 at. pct Cr, 0.9 at. pct Fe, and 0.0044 at. pct Ni.

The paraequilibrium solubility of carbon predicted by Eq. [1] is impressive: 5.5 at. pct at 750 K. The equilibrium solubility, in contrast, is only  $2.1 \cdot 10^{-4}$  at. pct at this temperature.

How do the calculated paraequilibrium solubilities compare with experimental data? The most illuminating data are those of Williams in Figure 2.<sup>[6]</sup> He processed a suite of 316L stainless steels with activation procedures of various efficacies and carburized them together at 738 K for 24 hours. The most successful of these surface activations led to a surface carbon concentration of  $\sim 12$  at. pct, as determined by glow discharge optical emission spectroscopy

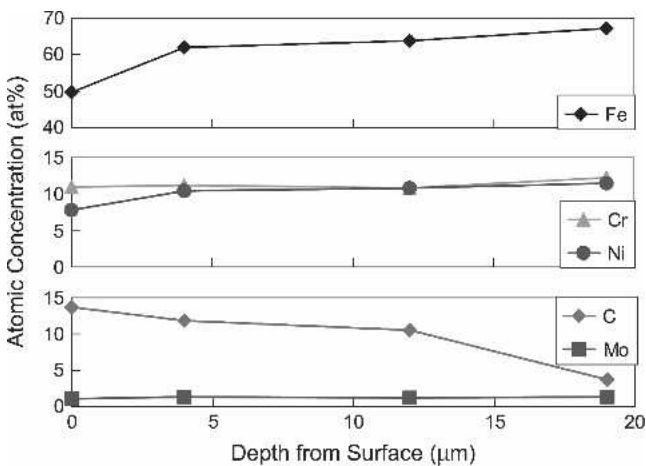


Fig. 4—ESCA (XPS) depth profiles showing the near-surface concentrations in a 316 stainless steel subjected to an optimized, single low-temperature carburization cycle. A suite of identical samples were electropolished to the indicated depths.

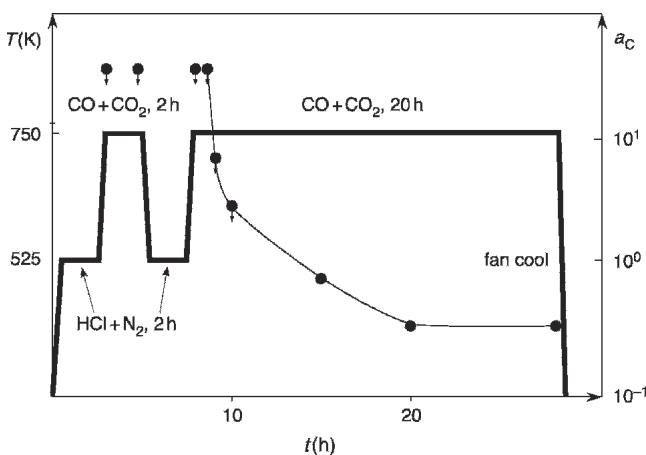


Fig. 5—Low-temperature activation/carburization process used by the Swagelok Company. This procedure was used for the sample of Figure 4. The downward arrows indicate ambients in which the calculated carbon activity,  $a_C$ , is greater than unity, implying possible sooting.

(GDOES), and a concomitant Vickers surface hardness of 1200. We have confirmed this high level of surface carbon content on similar samples provided by the Swagelok Company by a variety of experimental techniques, including electron spectroscopy for chemical analysis (ESCA, also known as XPS), X-ray energy-dispersive spectroscopy (XEDS) in a scanning electron microscope,<sup>[2]</sup> precision lattice parameter measurements,<sup>[2,12]</sup> and electron microprobe analysis.<sup>[18]</sup> Figure 4 presents the ESCA results.\*

\*Prior to low-temperature carburization, the surface of the Swagelok specimens was activated using gaseous HCl. The entire activation/carburization procedure is shown schematically in Figure 5. The Swagelok process involves carbon activities,  $a_C$ , more than 1 during the activation, but for the final 14 hours of the low-temperature carburization cycle,  $a_C$  is decreased ultimately to 0.32.

The data of Sun *et al.*<sup>[4]</sup> and Aoki *et al.*<sup>[5]</sup> confirm the general trend of Williams' data for other 316 samples, although neither group plotted hardness *versus* carbon content. Sun *et al.*<sup>[4]</sup> applied a plasma carburization procedure\*\*

\*\*Experimental details in this work are sparse. They reported, "A wide range of processing temperatures between 300 and 600 °C and times between 3 and 40 h have been employed."

and achieved surface carbon concentrations up to 10.5 at. pct. Aoki *et al.*<sup>[5]</sup> used  $NF_3$  activation and gaseous carburization using a  $N_2/CO/H_2$  ambient 743 K and found surface carbon levels up to 9.5 at. pct. Clearly, the CALPHAD parameters taken from Reference 17 do not accurately predict the high paraequilibrium solubilities that are observed experimentally.

A second route to evaluate the paraequilibrium solubility of carbon in the model austenitic stainless steel is available from the comprehensive study by Natesan and Kassner (henceforth N-K),<sup>[19]</sup> who measured the solubility of carbon in Fe-Ni and Fe-Cr-Ni alloys and modeled their findings using the Wagner interaction coefficient formalism. Their equation for the activity of carbon in austenite (applicable in principle to Cr contents up to 22 wt pct) can be expressed as

$$\ln[a_C] = \ln\left[\frac{X_C}{1-X_C}\right] + \ln[{}^0\gamma_C] + \varepsilon_C^C\left(\frac{X_C}{1-X_C}\right) + \varepsilon_C^{Ni}X_{Ni} + \varepsilon_C^{Cr}X_{Cr} + \rho_C^{Cr}X_{Cr}^2 \quad [3]$$

Here,  ${}^0\gamma_C$  represents the activity coefficient for carbon at infinite dilution,  $\varepsilon_C^i$  are first-order interaction coefficients, and  $X_i$  are atomic fractions. To accurately account for the high concentration of Cr, Eq. [3] also contains a term quadratic in  $X_{Cr}$ , with  $\rho_C^{Cr}$  being the second-order interaction coefficient. The paraequilibrium solubility of carbon in austenite is obtained by solving Eq. [3] for  $X_C$  with  $a_C = 1$ , using the temperature-dependent interaction coefficients from Reference 19. This second paraequilibrium solvus line is also plotted in Figure 3 (the curve marked "N-K graphite") and agrees with the CALPHAD calculation at 1300 K. This temperature is in the middle of the range where the experimental data that determine the coefficients in the thermodynamic models were obtained. At lower temperatures, however, the N-K paraequilibrium solubility suggests much greater carbon levels than the CALPHAD approach,

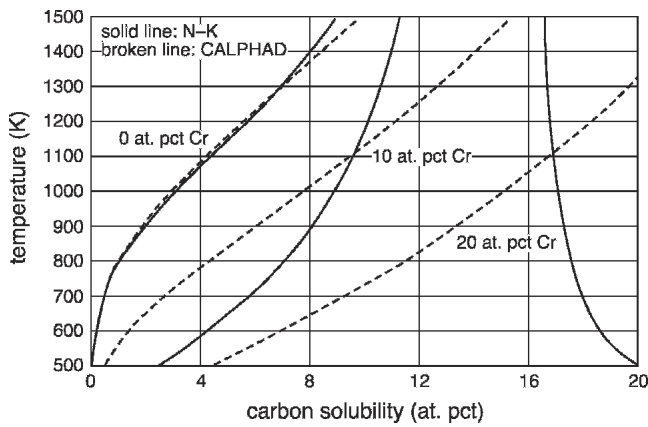


Fig. 6—Carbon solubility in austenitic alloys with Fe:Cr atom fraction ratios maintained at 100:0, 90:10, and 80:20, plotted as a function of temperature, calculated using Equations [4] to [7].

≈11 at. pct at 740 K, which is in much better agreement with experimental data (the maximum carbon contents shown in Figure 2).

To better compare the two approaches, it is useful to recast Eq. [1] into a Wagnerian-type formulation to compare with the N-K model. For binary Fe-carbon alloys, and using numeric values taken from References 17 and 19, the carbon activities of the two approaches are given by Eqs. [4] (N-K) and [5] (CALPHAD).

$$\ln[a_C] = \ln\left[\frac{X_C}{1-X_C}\right] - 1.845 + \frac{5100K}{T} + \left(11.92 - \frac{6330K}{T}\right) \frac{X_C}{1-X_C} \quad [4]$$

$$\ln[a_C] = \ln\left[\frac{X_C}{1-2X_C}\right] - 1.910 + \frac{5104K}{T} + \left(\frac{8362K}{T}\right) \frac{X_C}{1-X_C} \quad [5]$$

The absence of the factor 2 in the denominator of the first term in Eq. [4] is due to N-K not properly evaluating the ideal entropic factor for an interstitial solute. Nevertheless, evaluation of the carbon solubility in austenite as a function of temperature using these two equations yields essentially the same binary solvus, as shown in Figure 6 (the lines marked 0 pct Cr).

Comparable expressions for ternary *fcc* Fe-Cr-carbon alloys are

$$\ln[a_C] = \ln\left[\frac{X_C}{1-X_C}\right] - 1.845 + \frac{5100K}{T} + \left(11.92 - \frac{6330K}{T}\right) \frac{X_C}{1-X_C} + \left(24.2 + \frac{38400K}{T}\right) X_{Cr} + \left(-96.8 + \frac{84800}{T}\right) X_{Cr}^2 \quad [6]$$

and

$$\ln[a_C] = \ln\left[\frac{X_C}{1-2X_C}\right] - 1.910 + \frac{5116K}{T} + \left(\frac{8340K}{T}\right) \frac{X_C}{1-X_C} + \left(3.76 - \frac{17360K}{T}\right) \frac{X_{Cr}}{1-X_C} + \left(-1.288 + \frac{9733K}{T}\right) \left(\frac{X_{Cr}}{1-X_C}\right)^2 + \frac{399K}{T} \left(\frac{X_{Cr}}{1-X_C}\right)^3 + \left(1.64 - \frac{5459K}{T}\right) \frac{X_C X_{Cr}}{(1-X_C)^2} \quad [7]$$

N-K (Eq. [6]) do not provide the higher-order terms used in the CALPHAD approach (the last two terms of Eq. [7]), but these latter terms have only a modest effect on the calculated activities.

The paraequilibrium carbon solubilities derived from Eqs. [6] and [7] are shown in Figure 6 for hypothetical ternary austenitic alloys with Fe:Cr ratios maintained at 90:10 and 80:20 (the lines marked 10 pct and 20 pct Cr, respectively). The large differences in the temperature dependence of the exothermic Cr-carbon interaction parameters between Eqs. [6] and [7] cause commensurate changes in the paraequilibrium carbon solubilities. This effect is so marked that the N-K prediction for the Fe-20 pct Cr alloy shows retrograde carbon solubility. (The endothermic contribution of Ni in the model Fe-18Cr-12Ni austenitic alloy discussed previously prevented retrograde paraequilibrium carbon solubility.)

The comparable set of equations for the quaternary Fe-Cr-Ni-carbon system has not been included here, as it is clear that the major discrepancy between CALPHAD and N-K shown in Figures 3 and 6 arises from the Cr-carbon interaction terms in Eqs. [6] and [7], which in Lee's CALPHAD assessment<sup>[17]</sup> are insufficiently exothermic at low temperatures.

It is of interest to discuss the origin of the discrepancy. The first CALPHAD assessment of the Fe-Cr-Ni-carbon system was by Hillert and Qui,<sup>[20]</sup> who considered N-K's data in detail in their formulation of a consistent set of CALPHAD parameters. (Lee's assessment<sup>[17]</sup> was essentially a correction to Hillert and Qui.) N-K stated in their abstract and in the text that carbide precipitates were observed in their higher-Cr-content alloys containing 8 wt pct Ni equilibrated at low temperatures and high carbon activities, but they provided no details and did not consider this further in evaluating the data that led to Eq. [6]. Because of this, Hillert and Qui (and subsequently Lee) took a conservative approach and did not use N-K's higher-Cr-content alloys in establishing the parameters to be used in Eq. [1]. Figure 6 and Eqs. [6] and [7] reveal that this leads to a temperature dependence for the Cr-carbon interaction that is not appropriate at low temperatures, and to an underestimation of the paraequilibrium carbon solubility in the model Fe-18Cr-12Ni austenitic alloy. The standard CALPHAD database, which includes Lee's parameters for the Fe-Cr-Ni-carbon system,<sup>[21]</sup> appears to be in need of modification, particularly in the temperature dependence of the Cr-carbon interaction parameters.

Of course, the parameters of Eq. [6] cannot be used uncritically because of the acknowledged presence of

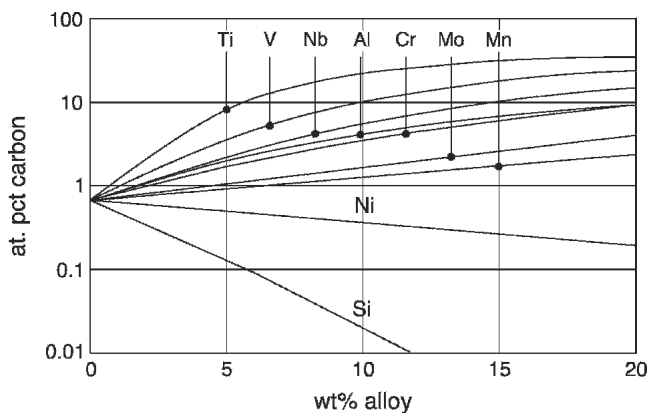


Fig. 7—Carbon solubility in Fe-based austenitic alloys at 750 K as a function of ternary alloy additions under paraequilibrium conditions.

carbides in N-K's higher-Cr-content alloys. The seriousness of this omission is not clear. Although no discussion of the detection limits for carbide formation was provided by N-K, the agreement between the N-K paraequilibrium carbon solubility shown in Figure 3 and the maximum carbon levels achieved by paraequilibrium carburization (Figure 2) suggests that N-K's parameters can be accepted as a zero-order estimate of the Cr-carbon interaction, and that only modest carbide formation must have occurred in their experiments.

Given the extraordinary properties<sup>[2,4,5,6]</sup> of 316L stainless steels containing colossal carbon levels, and notwithstanding the fact that the CALPHAD database underestimates the paraequilibrium carbon solubility by at least a factor of 2, it was of interest to assess the effect of other substitutional solutes on the paraequilibrium carbon solubility. The strong carbide forming elements (*e.g.*, Ti, V, and Nb) all increase the paraequilibrium carbon solubility at 750 K compared to the 0.68 at. pct solubility of carbon in unalloyed Fe, as shown in Figure 7. Only Ni and Si decrease the carbon solubility. The data of Figure 7 suggest interesting alloy development strategies for further enhancing the properties of austenitic stainless steels.

The greatly increased solubility of an interstitial solute under paraequilibrium conditions was observed by Darken in a ferrite matrix nearly 50 years ago,<sup>[22]</sup> although the term "paraequilibrium" was not used. As discussed by Swalin,<sup>[23]</sup> Darken's work revealed a significant paraequilibrium solubility of nitrogen in *bcc* Fe-Al alloys when equilibration with NH<sub>3</sub>-H<sub>2</sub> atmospheres was conducted at a temperature low enough that AlN could not form. It is surprising that incorporation of high levels of interstitials such as nitrogen and carbon under paraequilibrium conditions has not received more attention in the intervening years.

### III. PARAEQUILIBRIUM CARBIDE FORMATION

Our earlier work<sup>[13]</sup> showed that 316L austenitic stainless steels that had been carburized several times using the cycle shown in Figure 5 (to produce thicker cases) contained carbides that had apparently formed during the multiple carburization cycles. Two different carbides were found. The more abundant carbide has stoichiometry M<sub>5</sub>C<sub>2</sub> (the Hägg or  $\eta$  carbide), the less abundant M<sub>7</sub>C<sub>3</sub> stoichi-

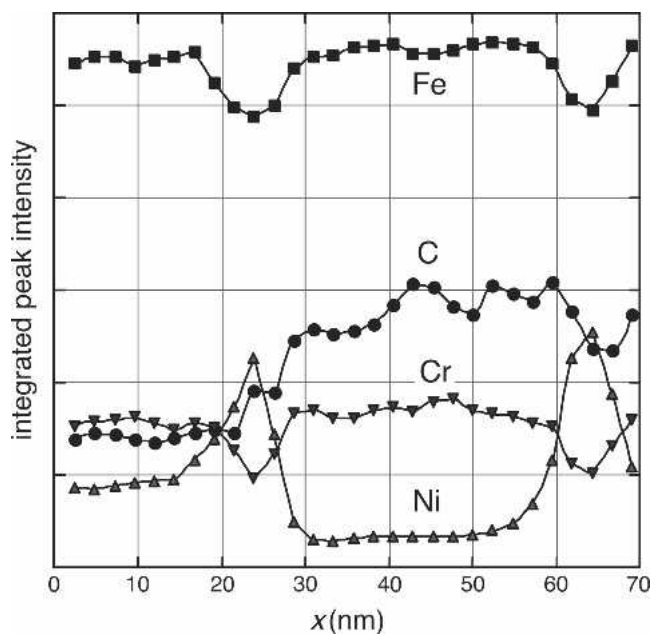


Fig. 8—XEDS line scan across a lathe-shaped particle of Hägg carbide in a 316 austenitic stainless steel that was subjected to 10 low-temperature carburization cycles of the type shown in Figure 5.

ometry. We have also calculated the paraequilibrium carbon solubility in austenite when paraequilibrium carbide formation has occurred—that is, in the presence of a carbide with the same Fe:Cr:Ni ratio as the austenite matrix, formed in a "partitionless" manner with regard to substitutional elements. Ignoring again the problems with Lee's CALPHAD parameters, the paraequilibrium carbon solubility in austenite containing partitionless M<sub>23</sub>C<sub>6</sub> is shown in Figure 3 (the curve marked "CALPHAD M<sub>23</sub>C<sub>6</sub> paraequilibrium"). The carbon solubility in this case is leaner than the carbon solubility in paraequilibrium with graphite. (The data required to evaluate the paraequilibrium solubility in austenite in the presence of partitionless M<sub>5</sub>C<sub>2</sub> were not available.) The increased austenite solubility, compared to the equilibrium solubility in the presence of M<sub>23</sub>C<sub>6</sub>, follows from the fact that the free energy of carbides containing 18 wt pct Cr and 12 wt pct Ni is much higher than that of the high-Cr, low-Ni equilibrium carbides. Our observation that the M<sub>5</sub>C<sub>2</sub> structure forms preferentially must be due to its stability relative to other partitionless carbides with M<sub>23</sub>C<sub>6</sub>, M<sub>7</sub>C<sub>3</sub>, M<sub>3</sub>C, and M<sub>2</sub>C stoichiometries and/or the relative ease of nucleation of M<sub>5</sub>C<sub>2</sub> relative to these other possible partitionless carbides.\*

\*It is possible that the M<sub>7</sub>C<sub>3</sub> carbides we observed earlier<sup>[13]</sup> had formed *in situ* from M<sub>5</sub>C<sub>2</sub> carbides, but further work is needed to understand paraequilibrium carbide formation.

We have used analytical electron microscopy to determine the chemistry of the Hägg carbides formed under paraequilibrium conditions. Figure 8 displays results from an EDS line scan across a particle of Hägg carbide embedded in a low-temperature carburized 316 austenitic stainless steel matrix. The relative numbers of counts in the Fe, Cr, Ni, and carbon peaks as a function of position are shown. The carbides appear to form in a *near*-partitionless manner,

the Ni-carbon interaction being sufficiently endothermic that the Ni content of the carbide is reduced by approximately a factor of 2, with the rejected Ni accumulated at the austenite/carbide interfaces. The relative difficulty of forming paraequilibrium carbides renders the carburization cycle shown in Figure 5, which is designed to provide hardened single-phase austenite, an industrially robust process.

#### IV. HARDNESS ACHIEVED BY PARAEQUILIBRIUM CARBURIZATION

Low-temperature carburized austenitic stainless steels possess remarkable mechanical and electrochemical properties.<sup>[2,4,5,6]</sup> Although not a principal focus of this paper, the hardness of the higher-carbon-content materials shown in Figure 2 is worthy of comment. A surface Vickers hardness of 1200 HV, equivalent to a Rockwell C hardness of 72, is unprecedented for austenitic stainless steels, particularly as this hardness is *not* accompanied by a significant loss of ductility.<sup>[2]</sup> What is surprising is the concave nature of the hardness-carbon content curve in Figure 2. It is only when carbon levels larger than 8 to 10 at pct are realized that superhardness, equivalent to those found in martensitic steels, is achieved. Understanding this effect is a research topic in its own right.

The exceptional surface hardness of low-temperature-carburized austenitic stainless steel is accompanied by improved wear resistance,<sup>[2,4,5]</sup> improved high-cycle fatigue resistance<sup>[2]</sup> (because of the surface residual compressive stresses accompanying the carbon concentration profile<sup>[2,12]</sup>), and probably improved resistance to stress-corrosion cracking. The multiple benefits of paraequilibrium carburization for austenitic stainless steels, which can be imparted to finished components by a low-cost, conformal, industrially relevant process, bodes well for the use of carburized stainless steels in new and demanding applications and improved performance of these materials in existing applications.

#### V. SUMMARY AND CONCLUSION

Low-temperature carburization of austenitic stainless steels leads to exceptional surface properties, enabled by carbon solubilities of up to 12 at. pct for 316-type alloys—a *colossal* carbon supersaturation. We have investigated the thermodynamic principles of this phenomenon. The key to this colossal super-saturation is paraequilibrium, a state in which interstitially dissolved carbon diffuses to equilibrate the chemical potential of carbon, while substitutional solutes are immobile.

The paraequilibrium carbon solubility was predicted using the CALPHAD approach. Using the interaction

parameters in the present CALPHAD database,<sup>[17]</sup> we obtained a carbon concentration more than  $2 \cdot 10^4$  times larger than the corresponding equilibrium concentration at the processing temperature. However, this prediction is still a factor of 2 too low compared to experimental data. The discrepancy arises because the CALPHAD interaction parameters for the Cr-carbon interaction are insufficiently exothermic at the low temperatures used for paraequilibrium carburization.

#### ACKNOWLEDGMENTS

This article is dedicated to Mats Hillert on the occasion of his 80th birthday. The authors thank Peter Williams, Sunniva Collins, and Steven Marx of the Swagelok Company for numerous fruitful discussions. Financial support for the work was provided by the Swagelok Company, the DOE “Industrial Materials of the Future” Program, and the Office of Naval Research.

#### REFERENCES

1. *Stainless Steel 2000 Thermochemical Surface Engineering*, edited by T. Bell and K. Akamatsu, Maney Publishing, London, 2001.
2. G. Michal, F. Ernst, H. Kahn, Y. Cao, F. Oba, and A.H. Heuer: *Acta Mater.*, in press.
3. B. Weiss and R. Stickler: *Metall. Trans.*, 1972, vol. 3, p. 851.
4. Y. Sun, X. Li, and T. Bell: *Surf. Eng.*, 1999, vol. 15, p. 49.
5. K. Aoki, T. Shirahata, M. Tahara, and K. Kitano: in *Stainless Steel 2000*, edited by T. Bell and K. Akamatsu, Maney Publishing, London, 2001, p. 389.
6. P. Williams: Swagelok Company, private communication.
7. C. Wells and R.F. Mehl: *Trans. Metall. Soc.*, 1940, vol. 140, p. 279.
8. W. Batz, R.F. Mehl, and C. Wells: *Trans. Metall. Soc.*, 1950, vol. 188, p. 553.
9. W.J. Liu, J.K. Brimacombe, and E.B. Hawbolt: *Acta Metal. Mater.*, 1991, vol. 39, p. 2373.
10. A. Hultgren: *Trans. ASM*, 1947, vol. 39, p. 915.
11. M. Hillert: *Jernkontorets Ann.*, 1952, vol. 136, p. 25.
12. Y. Cao, F. Ernst, and G. Michal: *Acta Mater.*, 2003, vol. 51, p. 4171.
13. F. Ernst, Y. Cao, and G. Michal: *Acta Mater.*, 2004, vol. 52, p. 1469.
14. E.C. Bain and H. Paxton: *Alloying Elements in Steel*, American Society for Metals, Metals Park, OH, 1961, pp. 125-28.
15. G. Krauss: in *Hardenability Concepts with Applications to Steel*, edited by D.V. Doane and J.S. Kirkaldy, AIME, Warrendale, PA, 1978, pp. 229-48.
16. M. Cohen: *Trans. TMS-AIME*, 1962, vol. 224, p. 638.
17. B.J. Lee: *CALPHAD*, 1992, vol. 16, p. 121.
18. N. Yang: Sandia Laboratories, private communication.
19. K. Natesan and T.F. Kassner: *Metall. Trans.*, 1973, vol. 4, p. 2557.
20. M. Hillert and C. Qui: *Metall. Trans.*, 1991, vol. 22A, p. 2187.
21. L. Kaufman: personal communication.
22. L.S. Darken: in *The Physical Chemistry of Metallic Solutions and Intermetallic Compound*, Vol II, Chemical Publishing Co., New York, NY, 1960, p. 80.
23. R.A. Swalin: *Thermodynamics of Solids*, John Wiley and Sons, New York, NY, 1962, p. 235.